Adsorptive Removal of Iodate Oxyanions from Water using a Zr-based Metal–Organic Framework

Christopher Copeman,[a] Hudson A. Bicalho,[a] Maxwell W. Terban,[b] Diego Troya,[c] Martin Etter,[d] Paul L. Frattini,[e] Daniel W. Wells,[e] Ashlee J. Howarth*[a]

A Zr_6-based metal–organic framework (MOF), MOF-808, is investigated for the adsorptive removal of IO_3^- from aqueous solutions, due to its high surface area and abundance of open metal sites. The uptake kinetics, adsorption capacity and binding mode are studied, showing a maximum uptake capacity of 233 mg/g, the highest reported by any material.

Iodine is generally found in the environment as the stable isotope ^{127}I. It is an essential element for animals and humans as it acts as a key component of thyroid hormones used to regulate growth, development, and metabolism.[1] Radioisotopes of iodine such as ^{129}I and ^{131}I, on the other hand, are produced as fission products in the generation of nuclear power and can enter the environment through the mishandling of spent nuclear fuel.[2] ^{129}I is a particular concern, because it is extremely long-lived with a half-life of 15.7 million years.[3] Radioisotopes of iodine exist in aqueous environments as iodide, I^-, and its oxyanion, iodate, IO_3^-.[4] Both species are readily soluble in water and can easily enter the body through the ingestion of contaminated water or crops, as well as via inhalation.[5,6] Exposure to radioisotopes of iodine can lead to thyroid pathologies,[7] including issues with hormone production and cancer.[8] While materials and technologies have been studied for the removal of iodine species from water, there is often a focus on I^-,[9] and the study of MOFs as sorption platforms for iodine has been heavily focused on adsorption of gaseous I_2.[10] Current materials for IO_3^- removal are often limited by slow kinetics or low uptake capacities, resulting in large amounts of sorbent being required for sufficient uptake.[11,12]

Metal–organic frameworks (MOFs) are coordination polymers consisting of metal centers connected to one another by organic ligands to form networks that are often crystalline and highly porous.[13] The metal nodes can be single metal ions, chains, or clusters, while the organic ligands, or linkers, can be di-, tri, or tetratopic.[14] Due to the vast array of metal and organic linker combinations, and a multitude of accessible topologies, MOFs can be designed to have large surface area, permanent porosity, and high thermal and chemical stability.[15] As a result, MOFs have been proposed for a diverse array of applications including gas storage,[16] catalysis,[17] water treatment,[18] sensing,[19] and more.[20] Zirconium-based MOFs, constructed using a Zr_6 octahedron cluster as the metal node, take advantage of the strong Zr(IV)-O bond between the metal center and multitopic carboxylate linkers, resulting in robust materials that are stable in aqueous conditions.[21] Additionally, they can possess accessible metal sites, capped by labile –OH and $–OH_2$ ligands, that allow for the adsorption of a variety of guest molecules. Zirconium cluster-based MOFs have been studied previously as adsorbents for the removal of oxyanions

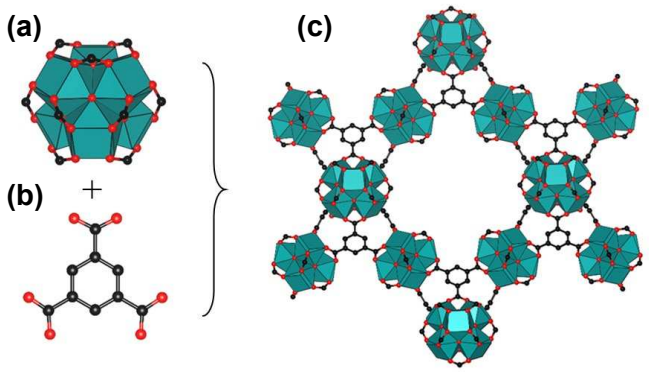

Figure 1 Zr_6 clusters (a) and 1,3,5-benzenetricarboxylate (b) are combined to produce the 6-connected MOF-808 (c).

a. *Department of Chemistry and Biochemistry, and Centre for NanoScience Research, Concordia University, 7141 Sherbrooke St W., Montreal, QC, H4B 1R6, Canada. E-mail: ashlee.howarth@concordia.ca.*
b. *Max Planck Institute for Solid State Research, Heisenbergstraße 1, 70569 Stuttgart, Germany*
c. *Department of Chemistry, Virginia Tech, Blacksburg, Virginia 24061, United States*
d. *Deutsches Elektronen-Synchrotron DESY, Notkestraße 85, 22607, Hamburg, Germany*
e. *Electric Power Research Institute Inc., 3420 Hillview Ave, Palo Alto, CA 94304, United States*

such as selenate, selenite,[22, 23] sulfate,[24] pertechnetate,[25] and antimonate[26] from water.

MOF-808 is a Zr_6-cluster-based MOF with 6-connected nodes bridged by the commercially available, tritopic, 1,3,5-benzenetricarboxylate linker (Figure 1).[27] MOF-808 is well suited towards wastewater remediation due to its high thermal and chemical stability (stable in solutions with pH ranging from 1-10).[28] Of the possible 12 metal node binding sites, only 6 are occupied by structural organic linkers in the **spn** topology of MOF-808, leaving 6 available to interact with adsorbate molecules, leading to the potential for high uptake capacity of guests.[27]

MOF-808 is synthesized under solvothermal conditions using $ZrOCl_2 \cdot 8H_2O$ and 1,3,5-benzenetricarboxylic acid in DMF with formic acid modulator at 120 °C. To ensure that the 6 nodal sites are accessible for oxyanion adsorption, the as-synthesized MOF is soaked in 0.1M HCl to remove the formate capping ligands leftover from synthesis. Powder X-ray diffraction (PXRD) confirms that the MOF is phase pure and crystalline after the removal of formate capping ligands (Figure S1) and ^{1}H NMR spectroscopy shows the disappearance of the formate proton at 7.92 ppm (Figure S2). N_2 gas adsorption analysis performed on MOF-808 shows the expected Type 1b isotherm, with a Brunauer-Emmett-Teller (BET) area of 2020 m^2/g and pore diameters of 10 and 18 Å (Figure S3), consistent with previous reports. Scanning electron microscopy images show the expected octahedral morphology, with crystallite sizes of approximately 5 µm (Figure S4).

To evaluate MOF-808 as a potential candidate for the adsorption of iodate, 2.5 mg of MOF-808 was exposed to solutions of potassium iodate with concentrations equivalent to exposures of 2-7 iodate anions per metal node of MOF (41-287 ppm). The MOF was submerged in the solution for 72 hours, resulting in iodate uptake between 0.95 per node and 1.93 per node for exposures of 2 and 7 iodate equivalents, respectively (Table S1). This translates to between 134 and 286 mg of iodate per gram of MOF-808, indicating that the MOF has a high gravimetric capacity for iodate adsorption.

Given the promising uptake of iodate in MOF-808 observed after 72 hours, the kinetics of the adsorption process were probed by exposing 2.5 mg of MOF-808 to 10 mL solutions of 1, 1.5, 2, 2.5 and 3 iodate anions per node (41, 61.5, 82, 102.5, 123 ppm respectively) (Figure 2a, Figures S5-9). The amount (q) of iodate adsorbed in mg/g of MOF was determined using equation 1.

Equation 1: $q = (C_i - C_f) \times V/m$

where C_i is the initial concentration (ppm), C_f is the final concentration (ppm), V is the volume of the iodate solution (L), and m is the mass of MOF-808 (g). In all cases, steep uptake is observed within the first few minutes of exposure of MOF-808 to the iodate solution, with uptake continuing to increase until reaching a plateau between 48-72 hours. The maximum adsorption capacity, Q, was calculated by fitting the data to the Langmuir adsorption model (Figure 2b, Figure S10), using equation 2.

Equation 2: $C_e/q_e = (1/Q)C_e + 1/K_LQ$

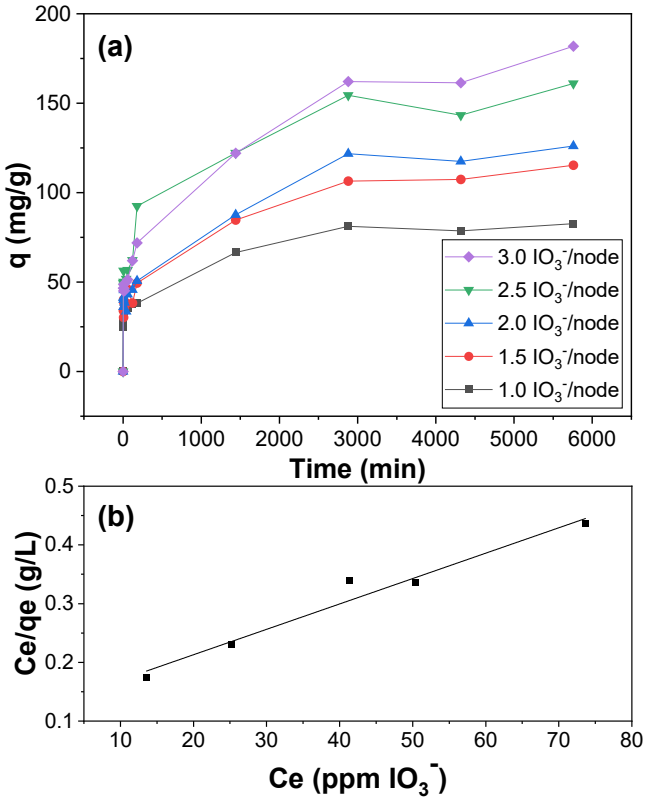

Figure 2. (a) Iodate uptake kinetics for MOF-808 when exposed to 1, 1.5, 2, 2.5, and 3 equivalents per node, 41.0, 61.5, 82.0, 102.5, 123.0 ppm KIO_3. (b) Langmuir plot summarizing the adsorption of iodate in MOF-808.

where Q is the equilibrium adsorption capacity (mg/g), C_e is the equilibrium concentration (ppm), q_e is the equilibrium uptake (mg/g), and K_L is the Langmuir adsorption constant. Q was determined to be 233 mg/g. This is the highest reported gravimetric iodate uptake to date, with other materials showing maximum adsorption capacities ranging from 0.01 – 170 mg/g (Table S2).

Depending on the application envisioned, the ability to reuse and recycle an adsorbent material may be an important factor, reducing the cost and amount of material required to remediate contaminated water. To assess the reusability of MOF-808, 10 mg of MOF-808 was loaded with iodate by exposing the MOF to a 1148 ppm solution of potassium iodate overnight resulting in uptake of 1.36-1.61 iodate/node. The following day, the iodate-loaded MOF-808 in the iodate solution was placed on a membrane filter in a glass microfiltration apparatus and the solution was passed through the filter by applying vacuum to the flask. The MOF-808 powder was then washed three times with 10 mL of water. 10 mL of 1% HCl was then passed through the MOF by controlled vacuum filtration over the course of 5 minutes. The MOF was then washed with water three times and placed in 10 mL of fresh 1148 ppm iodate solution overnight. The cycle was repeated three times for each, 1%, 3%, 5%, and 10% HCl. When using the 1% HCl solution for regeneration of MOF-808, a maximum of 0.40 iodate/node was removed from the MOF. The performance increased, however, with increasing acid strength. Washing the MOF with 3% HCl was found to remove a maximum of 0.55 iodate/node with a

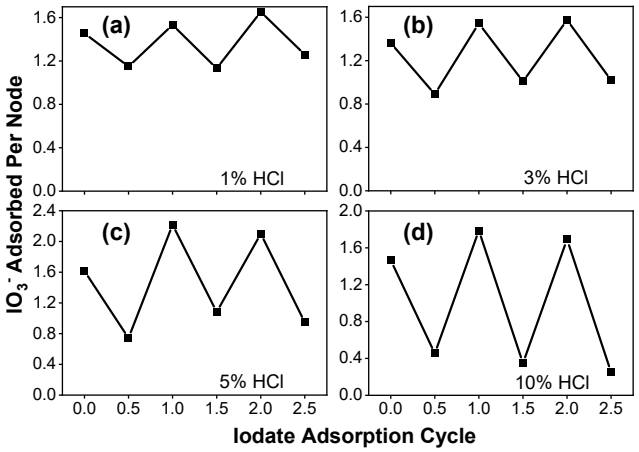

Figure 3. Adsorption and desorption cycles for iodate in MOF-808 IO_3^- using (a) 1%, (b) 3%, (c) 5%, and (d) 10% HCl to remove adsorbed iodate.

further increase when using 5% HCl to 1.15 iodate/node. Finally, using 10% HCl, the highest removal was obtained, with a maximum of 1.43 node equivalents removed, representing up to 85% removal of adsorbed iodate from the MOF. In between each acid wash, MOF-808 was exposed to a 1148 ppm solution of potassium iodate, and in each case, the maximum uptake was preserved over 2 subsequent adsorption-desorption cycles (Figure 3).

The mechanism of adsorption of iodate onto MOF-808 is supported by diffuse reflectance infrared Fourier transform spectroscopy (Figure S11) and differential pair distribution function (dPDF) analyses from total X-ray scattering data performed on samples of MOF-808 before and after iodate loading (Figure 4). A substantial decrease in the O–H stretch at

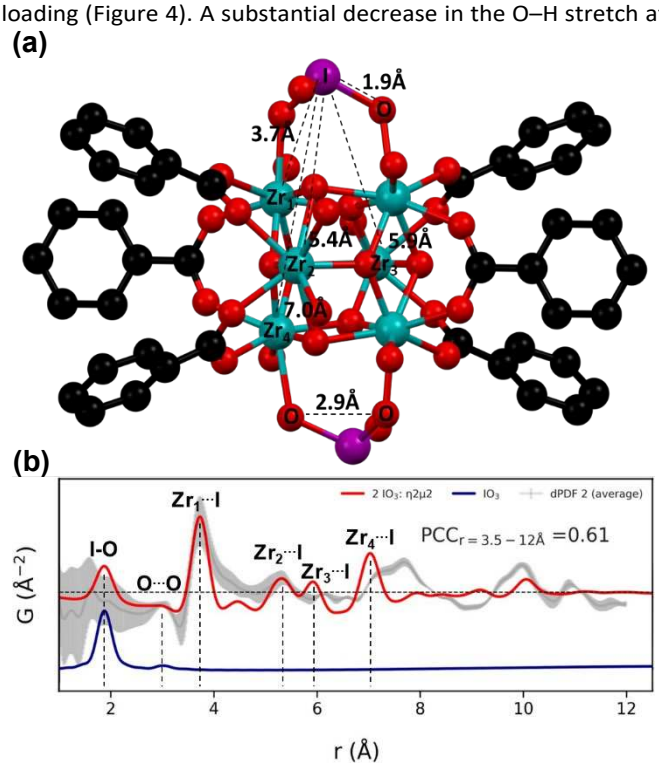

Figure 4. (a) MOF-808 node with bridging iodate ions. (b) Simulated differential pair distribution function (dPDF) of this DFT model (red trace) overlaid atop experimentally obtained dPDF of iodate-loaded MOF-808 from X-ray total scattering data (grey trace) alongside the PDF of unbound iodate (blue trace).

3674 cm^{-1} after iodate loading confirms that –OH ligands are replaced by iodate (Figure S11). Distances obtained via dPDF analysis are consistent with those determined by density functional theory (DFT) calculations for the optimized geometry of the Zr_6 cluster of MOF-808 with a bridging iodate. Atom-pair distances of 1.9 and 3.7 Å are observed after loading with iodate, corresponding to I–O and Zr–I, respectively. The signal is consistent with a binding mode where the iodate bridges two adjacent zirconium metal ions in the cluster, where peaks at larger distances are consistent with distances expected between iodine and successively further zirconium ions in the cluster. In contrast, models with monodentate binding through a single oxygen of iodate and chelate binding by two oxygen atoms of iodate to the same nodal zirconium ion both tended to predict severely mismatched pair distances between iodine and zirconium atoms (Figures S12-S28). The DFT calculations suggest that hydrogen bonding with bound water has a directive effect on the iodate orientation – thus parts of the dPDF not clearly indexed by the model may plausibly occur due to distributed orientations, e.g. by interaction with further water layers.

In order to test the integrity of MOF-808 after iodate adsorption, PXRD data were collected on MOF-808 before and after iodate loading as well as after regeneration using HCl (Figure 5a). PXRD confirms that crystallinity is maintained not

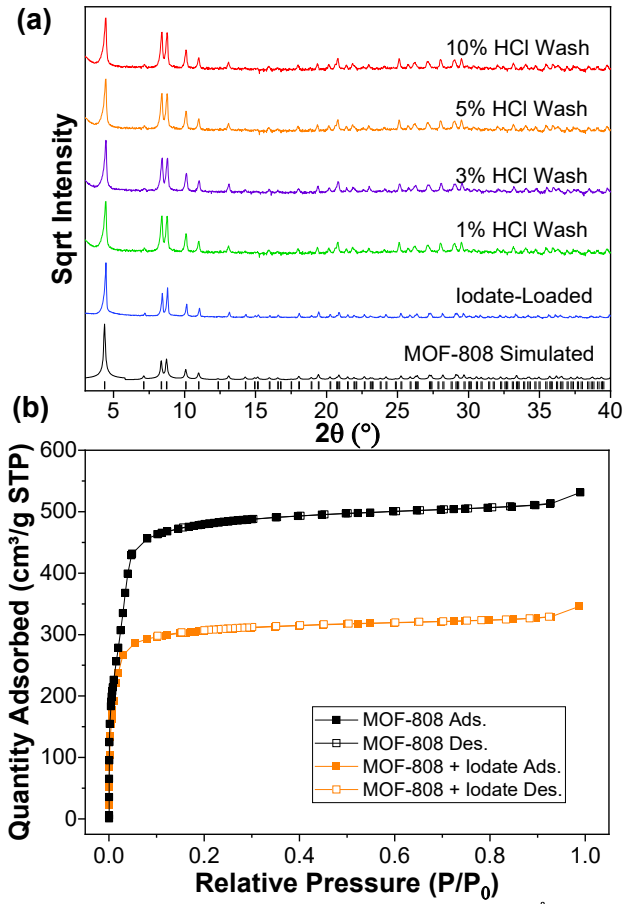

Figure 5. (a) Powder X-ray diffraction patterns (CuK_α, λ = 1.54178 Å) for MOF-808 including simulated, as-synthesized, and acid regenerated (1%, 3%, 5%, 10% HCl wash). (b) Nitrogen adsorption-desorption isotherms for MOF-808 before and after iodate loading.

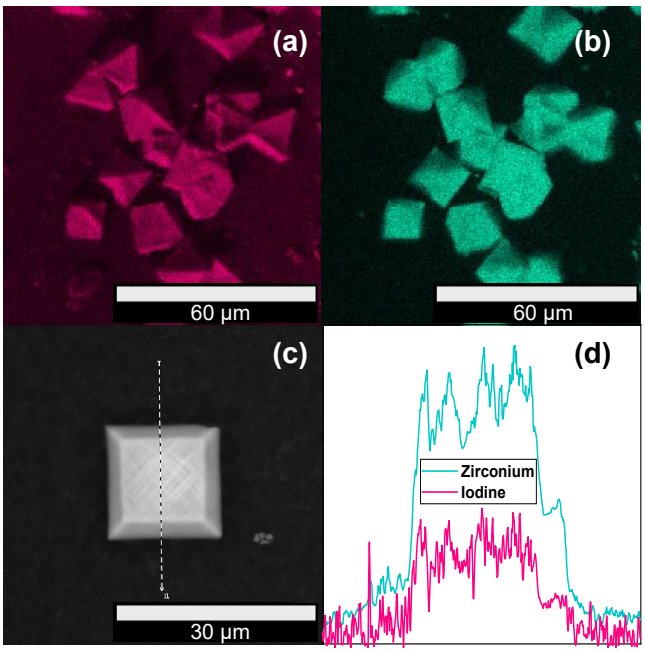

Figure 6. SEM images with EDS elemental mapping for iodine (a), and zirconium (b), and a MOF-808 crystallite (c), with SEM-EDS line scan analysis (d).

only after iodate adsorption but also after 3 regenerative washing steps with 1, 3, 5, or 10% hydrochloric acid. Retention of porosity is also confirmed by comparing the N_2 adsorption isotherms before and after iodate adsorption (Figure 5b). Both isotherms are Type 1b isotherms, with a reduction in BET area from 2020 m^2/g to 1300 m^2/g and a reduction in pore volume from 0.471 cm^3/g to 0.263 cm^3/g in the 18 Å pore (Figure S29). This decrease in surface area and pore volume is consistent with iodate uptake occurring primarily in the 18 Å pore.

Larger crystallites of MOF-808 were grown for easier visualization by electron microscopy. Scanning electron microscopy images show that the MOF-808 octahedral morphology is maintained after loading with Iodate (Figure 6). Furthermore, energy dispersive X-ray spectroscopy (EDS) elemental mapping and line scan analysis of iodate loaded MOF-808 crystallites shows iodine distributed evenly throughout the MOF crystallite (Figure 6).

In conclusion, MOF-808, a robust, water stable Zr_6-cluster based MOF was evaluated for the adsorption of iodate from water. MOF-808 is determined to have an exceptionally high uptake capacity of 233 mg/g, equivalent to 1.63 iodate anions per Zr_6-metal node. This high uptake arises from the presence of 6 –OH groups on the MOF metal node that act as adsorption sites for oxyanions. Additionally, iodate-loaded MOF-808 can be regenerated by washing with 10% HCl, removing over 80% of the bound iodate over three cycles and without affecting subsequent adsorption. Finally, iodate is shown to bind in a bridging fashion to two zirconium ions in the cluster node.

We acknowledge PR Donnarumma for assistance with molecular modelling, and Dr. Heng Jiang from CBAMS for his assistance with ICP-MS. AJH thanks EPRI and the CURC program for funding. We acknowledge DESY (Hamburg, Germany), a member of the Helmholtz Association HGF, for the provision of experimental facilities. Parts of this research were carried out at PETRA III beamline P02.1. Beamtime was allocated by an In-House contingent.

References

1 WHO. *Trace Elements in Human Nutrition and Health,* WHO, Geneva, 1996.
2 J. M. Gómez-Guzmán, E. Holm, N. Niagolova, J. M. López-Gutiérrez, A. R. Pinto-Gómez, J. A. Abril and M. García-León, *Chemosphere,* 2014, **108**, 76–84.
3 M. Eisenbud and T. F. Gesell, *Environmental Radioactivity from Natural, Industrial and Military Sources,* Academic Press, San Diego, 1997.
4 M. Fukui, Y. Fujikawa and N. Satta, *J. Environ. Radioact*., 1996, **31**, 199–216.
5 M. Murakami and T. Oki, *Chemosphere*, 2012, **87**, 1355–1360.
6 L. S. Lebel, R. S. Dickson and G. A. Glowa, *J. Environ. Radioact.,* 2016, **151**, 82–93.
7 J. R. Goldsmith, C. M. Grossman, W. E. Morton, R. H. Nussbaum, E. A. Kordysh, M. R. Quastel, R. B. Sobel and F. D. Nussbaum, *Environ. Health Persp.*, 1999, **107**, 303–308.
8 J. Robbins and A. B. Schneider, *Rev. Endocr. Metab. Disord*., 2000, **1**, 197–203.
9 (a) L. Hashemi and A. Morsali, *CrystEngComm*, 2012, **14**, 779–781. (b) X. Zhang, P. Gu, X. Li and G. Zhang, *Chem. Eng. J.,* 2017, **322**, 129–139. (c) X. Zhao, X. Han, Z. Li, H. Huang, D. Liu and C. Zhong, *Appl. Surf. Sci.,* 2015, **351**, 760–764.
10 P. Chen, X. He, M. Pang, X. Dong, S. Zhao and W. Zhang, *ACS Appl. Mater. Interfaces,* 2020, **12**, 20429–20439.
11 R. C. Moore, et. al. *Sci. Total Environ,* 2020, **716***,* 132820.
12 *Iodine Adsorption on Ion-Exchange Resins and Activated Carbons-Batch Testing.* Pacific Northwest National Laboratory, Richland, WA: 2014. PNNL-23730
13 H. Li, M. Eddaoudi, M. O'Keeffe, and O. M. Yaghi, *Nature,* 1999**, 402**, 276-279.
14 H. Furukawa, K. E. Cordova, M. O'Keeffe and O. M. Yaghi, *Science*, 2013, **341**, 1230444.
15 O. M. Yaghi, M. O'Keeffe, N. W. Ockwig, H. K. Chae M. Eddaoudi and J. Kim, *Nature*, 2003, **423**, 705-714.
16 S. Ma and H.-C. Zhou, *Chem. Commun.* 2010, **46**, 44-53.
17 L. Ma, C. Abney and W. Lin, *Chem. Soc. Rev.* 2009, **38**, 1248-1256.
18 A. J. Howarth, Y. Liu, J. T. Hupp and O. K. Farha, *CrystEngComm,* 2015, **17**, 7245-7253.
19 C. A. Bauer, T. V. Timofeeva, T. B. Settersten, B. D. Patterson, V. H. Liu, B. A. Simmons and M. D.Allendorf, *J. Am. Chem. Soc.*, 2007, **129**, 7136-7144.
20 P. Horcajada, C. Serre, G. Maurin, N. A. Ramsahye, F. Balas, M. Vallet-Regí, M. Sebban, F. Taulelle, and G. Férey, *J. Am. Chem. Soc.* 2008, **130**, 6774–6780.
21 J. H. Cavka, S. Jakobsen, U. Olsbye, N. Guillou, C. Lamberti, S. Bordiga, and K. P. Lillerud, *J. Am. Chem. Soc.,* 2008, **130**, 13850–13851
22 A. J. Howarth, M. J. Katz, T. C. Wang, A. E. Platero-Prats, K. W. Chapman, J. T. Hupp, and O. K. Farha, *J. Am. Chem. Soc*. 2015, **137**, 7488-7494.
23 R. J. Drout, A. J. Howarth, K. Otake, T. Islamoglu and O. K. Farha, *CrystEngComm*, 2018, **20**, 6140-6145.
24 A. J. Howarth, T. C. Wang, S. S. Al-Juaid, S. G. Aziz, J. T. Hupp, and O. K. Farha, *Dalton Trans.* 2015, **45**, 93–97.
25 R. J. Drout, K. Otake, A. J. Howarth, T. Islamoglu, L. Zhu, C. Xiao, S. Wang, and O. K. Farha, *Chem. Mater.* 2018, **30**, 1277–1284.
26 S. Rangwani, A. J. Howarth, M. R. DeStefano, C.D. Malliakas, A. E. Platero-Prats, K. W. Chapman, and O. K. Farha, *Polyhedron*, 2018, **151**, 338-343

27 H. Furukawa, F. Gándara, Y.-B. Zhang, J. Jiang, W. L. Queen, M. R. Hudson, and O. M. Yaghi, *J. Am. Chem. Soc.,* 2014, **136**, 4369-4381.
28 H.-Q. Zheng, C.-Y. Liu, X.-Y. Zeng, J. Chen, J. Lü, R.-G. Lin, R. Cao, Z.-J. Lin and J.-W. Su, *Inorg. Chem.*, 2018, **57**, 9096-9104.